



Adaptive and Rotating Non-local Weighted Joint Sparse Representation Classification for Hyperspectral Images

Jingwen Yan¹ , Hongda Chen¹ , Zixin Xie¹ , and Lei Liu²  

¹ Engineering College, Shantou University, Shantou 515063, China
jwyan@stu.edu.cn

² Medical College, Shantou University, Shantou 515063, China
wliulei@stu.edu.cn

Abstract. In this paper, we propose an adaptive and rotating non-local weighted joint sparse representation classification (ARW-JSRC) method for hyperspectral image (HSI). The proposed method aims at avoiding misclassification of the HSI pixels located around the boundaries of class and over-smoothed classification performance caused by the window-based technique used in joint sparse representation classification (JSRC). Since the window-based technique leads to the undesired classification result, an adaptive threshold based on the spectral angle between different classes and the rotated similar window replaced the traditional rectangular window are applied to sufficiently utilize the rich spectral-spatial signatures and alleviate this problem. Furthermore, a new weight formula that accurately reflects the spectral-spatial feature in HSI is applied to obtain more appropriate weights for HSI pixels in search window. Experimental results indicate that our method achieves great improvement in HSI classification, comparing to several widely used classification methods.

Keywords: Hyperspectral image classification · Adaptive threshold · Rotated similar window · Non-local weighted

1 Introduction

Since hyperspectral image (HSI) has hundreds of spectral bands, it has a higher spectral resolution comparing to other kinds of images, which improves its ability to distinguish different materials [1, 2]. Due to the each pixel in HSI corresponds to a spectral curve, it means that HSI classification is to assign each pixel a land-cover class based on their respective spectral information [3]. However, the high dimensional characteristic existing in HSI may cause the Hughes phenomenon [4], which poses a big challenge to the HSI classification.

Supported by the NSF of China (No. 61672335 and 61601276), and by Department of Education of Guangdong Province (No. 2016KZDXM012 and 2017KCXTD015).

Sparse representation (SR), a useful tool for high-dimensional signal processing, has been applied to HSI classification last few years. Related studies shown in [7–10] have displayed the achievement the SR based methods made. In 2011, Yi chen firstly applied the sparse representation classification (SRC) approach from other fields to HSI classification [5]. Meanwhile, the author proposed a joint sparse representation classification (JSRC) method rooting in the assumption that HSI pixels in a small area consist of similar material (same class). Though the JSRC has a better performance than SRC, there is a situation that not all HSI pixels can meet the assumption of JSRC. When the HSI pixel locates at regional edge, its neighboring pixels can not be guaranteed homogeneity. In order to reduce the interference of heterogeneous pixels in the neighborhood, Zhang in [6] proposed a non-local weighted joint sparse representation classification (NLW-JSRC) method. By assigning different weights to HSI pixels in search window according to the similarities between neighboring pixels and central pixel, the NLW-JSRC can improve the problem existing in JSRC. However, its calculation of weights can not fully consider the spatial information of the HSI and can not assign appropriate weights for pixels in search window.

In order to effectively reduce the interference of the heterogeneous pixels in the search window, we propose an adaptive and rotated non-local weighted sparse representation classification (ARW-JSRC) method. Compared with NLW-JSRC, our proposed method can provide more appropriate weight to every pixel in the search window. It uses a rotation transformation strategy to measure the similarity between the pixels in the search window, so as to make full use of the spatial information of the image. Then, a new weight calculation method is used to give more appropriate weight to each pixel in the search. The adaptive threshold involved in the weight formula is obtained by calculating the median of the maximum and minimum spectral angles of various training samples.

The remainder of this paper is organized as follows. The non-local weighted joint sparse representation classification is described in Sect. 2. Then, the adaptive and rotated non-local weighted joint sparse representation classification is introduced in Sect. 3. The experimental results and discussion are presented in Sect. 4. The conclusion is shown in Sect. 5.

2 Related Works

2.1 JSRC

In the JSRC, it is assumed that all neighboring HSI pixels in a small area can be approximately represented by the linear combination of a few common atoms with different coefficients. For any test HSI pixel $\mathbf{x}_i (i = 1, 2, \dots, N)$, let its search window size be set as $\sqrt{S} \times \sqrt{S}$, then the joint signal matrix $\mathbf{X} = [\mathbf{x}_1, \mathbf{x}_2, \dots, \mathbf{x}_S]$ can be represented as

$$\begin{aligned}
\mathbf{X} &= [\mathbf{x}_1 \ \mathbf{x}_2 \ \dots \ \mathbf{x}_S] \\
&= [D\boldsymbol{\alpha}_1 \ D\boldsymbol{\alpha}_2 \ \dots \ D\boldsymbol{\alpha}_S] \\
&= D \underbrace{[\boldsymbol{\alpha}_1 \ \dots \ \boldsymbol{\alpha}_i \ \dots \ \boldsymbol{\alpha}_S]}_{\boldsymbol{\Phi}} \\
&= D\boldsymbol{\Phi},
\end{aligned} \tag{1}$$

where $\boldsymbol{\Phi}$ is the sparse coefficient matrix with few nonzero rows and N is the number of test pixels in HSI. D is the over-complete dictionary consist of training pixels randomly selected from all classes in HSI with a certain proportion. Given the over-complete dictionary D and the joint signal matrix \mathbf{X} , the sparse matrix $\boldsymbol{\Phi}$ can be obtained as follow:

$$\boldsymbol{\Phi} = \arg \min \|\mathbf{X} - D\boldsymbol{\Phi}\|_F \quad \text{s.t.} \quad \|\boldsymbol{\Phi}\|_{row,0} \leq K, \tag{2}$$

where $\|\boldsymbol{\Phi}\|_{row,0}$ denotes the number of nonzero rows of $\boldsymbol{\Phi}$. Besides, the objective function (2) can be solved by the simultaneous orthogonal matching pursuit (SOMP) algorithm [11,12]. Once the sparse matrix $\boldsymbol{\Phi}$ is obtained, the test pixel \mathbf{x} can be labeled as follow

$$\begin{aligned}
Class(\mathbf{x}_i) &= \arg \min_{m=1,2,\dots,M} \|\mathbf{X} - D^m \boldsymbol{\Phi}^m\|_F, \\
i &= 1, 2, \dots, N,
\end{aligned} \tag{3}$$

where M is the number of classes in HSI. D^m is the sub-dictionary constructed by HSI pixels randomly selected from m th class.

2.2 NLW-JSRC

The author in [6] proposed the NLW-JSRC method that assigns appropriate weights to all neighboring pixels in search window based on the similarities between neighboring pixels and the central test pixel. The weight w_{ij} can be obtained mathematically by

$$w'_{ij} = (1 - (\frac{\|J(\mathbf{x}_i) - J(\mathbf{x}_j)\|}{\rho})^2)^2, \tag{4}$$

where $\|J(\mathbf{x}_i) - J(\mathbf{x}_j)\|$ denotes the similarity measure (euclidean distance) between the two HSI patches, which are sized as $so \times so$ and centered at the test pixel \mathbf{x}_j and the neighboring pixel \mathbf{x}_i , respectively. Parameter ρ is the $\max(\|J(\mathbf{x}_i) - J(\mathbf{x}_j)\|)$. Then, the weight scheme w'_{ij} is modified as follow:

$$w_{ij} = \begin{cases} 0 & 0 < w'_{ij} < w'_1 \\ w'_{ij} & w'_1 < w'_{ij} < w'_2 \\ 1 & w'_2 < w'_{ij} < 1 \end{cases}, \tag{5}$$

where w'_1 and w'_2 are two parameters applied to judge valid and invalid neighboring pixels.

With the joint consideration of (2) and (5), we get:

$$\begin{aligned} \Phi_{NLW} = \arg \min & \|XW_{NLW} - D\Phi\|_F, \\ \text{s.t.} & \|\Phi\|_{row,0} \leq K, \end{aligned} \tag{6}$$

where $W_{NLW} = \text{diag}(w_{i1}, w_{i2}, \dots, w_{im})$ is the non-local weighted matrix, and each weight can be get by (5). The sparse coefficient matrix Φ_{NLW} can be obtained as similar as the JSRC. Finally, the label for the test pixel x_i is given by minimizing the residual:

$$\begin{aligned} \text{Class}(x_i) = \arg \min_{m=1,2,\dots,M} & \|XW_{NLW} - D^m \Phi_{NLW}^m\|_F, \\ i = & 1, 2, \dots, N. \end{aligned} \tag{7}$$

3 Adaptive and Rotated Weighed Joint Sparse Representation Classification

Due to the NLW-JSRC can not consider the directionality of HSI spatial structure and the Turkey function failed to give appropriate weights. To make up for the deficiency of NLW-JSRC, the adaptive and rotated weighed joint sparse representation classification (ARWJSRC) is proposed. The proposed method can be divided into three parts, containing spectral angle, rotated similar window, weighed function.

3.1 Spectral Angle

In this paper, the spectral angle is used to measure the similarity between HSI pixels. Suppose that there is a search window centered at HSI pixel $x_i (i = 1, 2, \dots, N)$ with the size of $\sqrt{S} \times \sqrt{S}$ and pixel $x_j (j = 1, 2, \dots, S)$ is one of HSI pixels in search window, then the similarity between x_i and x_j can be written as

$$\theta_{ij} = \theta(\bar{x}_i, \bar{x}_j) = \frac{180^\circ}{\pi} \arccos \frac{\bar{x}_i \cdot \bar{x}_j}{\|\bar{x}_i\|_2 \|\bar{x}_j\|_2}, \theta_{ij} \in [0^\circ, 90^\circ], \tag{8}$$

where \bar{x}_i denotes the average of HSI pixels in similar window centered at x_i with the size of $\sqrt{s} \times \sqrt{s}$. It can be written as $\bar{x}_i = \frac{1}{s} \sum_{n=1}^s x_n (i = 1, 2, \dots, N)$. x_n is one of HSI pixels in similar window. Besides, \bar{x}_j is the average of HSI pixels in similar window centered at x_j with the size of $\sqrt{s} \times \sqrt{s}$.

The deficiency exiting in NLW-JSRC can not be solved if the similarity between x_i and x_j is measured directly as above. Because the calculation introduced above dose not consider the directionality of HSI spatial structure. Thus, the rotated similar window strategy is introduced in next subsection.

3.2 Rotated Similar Window Strategy

NLW-JSRC does not consider the directionality of HSI spatial structure and only calculate the Euclidean distance between two HSI patches. As considering the redundancy of image spatial information, we apply the rotated similar window technology instead of the traditional window technology to measure the similarity between neighboring pixel and the central. The rotated window method looks for the most similar structure through the rotation of the HSI patches so that the similarity between neighboring pixel and the central can be more accurately estimated. The Fig. 1 illustrates the process.

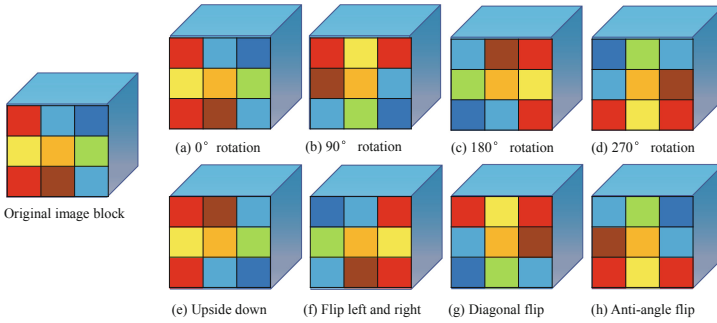


Fig. 1. The rotation measurement of similarity. The rotated similar window consists of the central pixel and its 8 neighboring pixels. Suppose that (a)–(d) are the HSI blocks obtained by rotating the original HSI block 0°, 90°, 180°, 270°, respectively. Besides, (e)–(h) are obtained by flipping the original HSI block upside down, left and right, diagonally, anti-diagonally, respectively. It is obvious that they have low similarities with it although (b)–(h) have the same spatial structure with the original HSI block. Because their directionality of HSI block are different from the original HSI block unless the (a). Thus, to find the most similar structure by rotating the HSI block is important to get a more accurate similarity measurement.

The following passage will mathematically introduce the specific process. Suppose that $\phi(\mathbf{x}_i)$ and $\phi(\mathbf{x}_j)$ respectively denotes the similar window centered at test HSI pixel \mathbf{x}_i and \mathbf{x}_j that is one of HSI pixels in the search window centered at \mathbf{x}_i . Then, the most similar structure $\hat{\phi}(\mathbf{x}_j)$ of \mathbf{x}_j with $\phi(\mathbf{x}_i)$ can be obtained by

$$\hat{\phi}(\mathbf{x}_j) = R_k[\phi(\mathbf{x}_j)] = \arg \min_{k=0,1,\dots,7} \|\phi(\mathbf{x}_i) - R_k[\phi(\mathbf{x}_j)]\|_F, \quad (9)$$

where $R_k[\bullet]$ denotes k th rotation or flip operation.

By getting $\hat{\phi}(\mathbf{x}_j)$ and $\phi(\mathbf{x}_j)$, their residual r_{min} , r_o with $\phi(\mathbf{x}_i)$ can be respectively expressed as

$$r_{min} = \|\hat{\phi}(\mathbf{x}_j) - \phi(\mathbf{x}_i)\|_F, \quad (10)$$

$$r_o = \|\phi(\mathbf{x}_j) - \phi(\mathbf{x}_i)\|_F. \tag{11}$$

Once the residuals r_{min} , r_o are obtained, a direction coefficient O can be got. The coefficient O can revise the spectral angle obtained by (9), which improve the measurement of similarity between HSI pixels. The coefficient O can be got by

$$O = \frac{r_{min}}{r_o}. \tag{12}$$

Then the revised spectral angle $\hat{\theta}_{ij}$ between the test pixel \mathbf{x}_i and any HSI pixel \mathbf{x}_j in search window centered at \mathbf{x}_i can be written as

$$\hat{\theta}_{ij} = \hat{\theta}(\bar{\mathbf{x}}_i, \bar{\mathbf{x}}_j) = \theta(\bar{\mathbf{x}}_i, \bar{\mathbf{x}}_j) \times O. \tag{13}$$

3.3 The Proposed Calculation of Weights

For any HSI pixel $\mathbf{x}_j(j = 1, 2, \dots, S)$ in the search window centered at a test pixel $\mathbf{x}_i(i = 1, 2, \dots, N)$, its weight w_{ij} in search window can be obtained by

$$w_{ij} = \frac{1}{1 + \left(\frac{\hat{\theta}_{ij}}{\theta_{th}}\right)^G}, \tag{14}$$

where G is the order that determined the decay rate of weight. The larger weight is, the more similar HSI pixels are. Vice versa. θ_{th} is a adaptive threshold which is got by calculating the median between the maximum and minimum of spectral angle between training samples. Here is its detailed process.

Given the training samples $\mathbf{X}_{train} = [\mathbf{X}_1, \dots, \mathbf{X}_i, \dots, \mathbf{X}_M]$, where $\mathbf{X} \in \mathbb{R}^{B \times N_i}$ is class i th training samples and N_i denotes the number of training samples in i th class. Then the average \bar{X}_i of class i can be written as

$$\bar{X}_i = \frac{1}{N_i} \sum_{n=1}^{N_i} \mathbf{x}_i^n, i = 1, 2, \dots, M. \tag{15}$$

After getting averages of all classes according to (15), their spectral angles $\theta_{ij} = \theta(\bar{X}_i, \bar{X}_j)$ can be obtained by (8) and sorted. The adaptive threshold θ_{th} is the median between the maximum θ_{max} and minimum θ_{min} selecting from the sorted spectral angles.

$$\theta_{th} = \frac{\theta_{max} + \theta_{min}}{2}. \tag{16}$$

3.4 Reconstruction and Classification

Suppose that there is a search window centered at test pixel \mathbf{x}_i with the size of $\sqrt{S} \times \sqrt{S}$ and all pixel in search window construct a joint signal matrix $\mathbf{X} = [\mathbf{x}_i^1, \mathbf{x}_i^2, \dots, \mathbf{x}_i^S]$, then a rotating weighted matrix $\mathbf{W}_{OW} =$

$diag(w_{i1}, w_{i2}, \dots, w_{iS})$ according to (14). Similar to (7), the sparse coefficient matrix Φ_{OW} can be obtained by

$$\Phi_{OW} = \arg \min \|XW_{OW} - D\Phi\|_F, s.t. \|\Phi\|_{row,0} \leq K, \quad (17)$$

In this paper, the SOMP algorithm is used to solve (17). Once the sparse coefficient matrix Φ_{OW} is got, the class of test HSI pixel \mathbf{x}_i can be determined by

$$\begin{aligned} Class(\mathbf{x}_i) &= \arg \min_{n=1,2,\dots,M} \|XW_{OW} - D_n\Phi_{OW}^n\|_F, \\ i &= 1, 2, \dots, N. \end{aligned} \quad (18)$$

4 Experiment and Discussion

In this paper, two data sets containing Indian Pines and Pavia University are used to evaluate the performance of the proposed method. Besides, several classical HSI classification algorithms are also used as contrasting methods to prove the superiority of our proposed method. The section can be divided into two parts: 1) experimental data; 2) experimental result and discussion.

In this paper, four evaluating indicators including the average accuracy (AA), the overall accuracy (OA), the kappa coefficient, and time were used to judge the classification results. In order to display superiority of the proposed method, several classical algorithms including SVM [14], SRC [5], JSRC [5], NLW-JSRC [6] are applied to compare with our method. Among those methods, SVM and SRC are pixel-wise classification algorithms which only takes into account the spectral information, whereas the rest is the spectral-spatial classification method.

The parameters of SVM are obtained by the 5-fold cross-validation technique. According to [5, 15], the sparsity level of all the sparse representation-based method mentioned in this paper was set to 3. If rising in sparsity level, it not only causes higher computational cost but also mislead the dictionary atoms from wrong classes to be selected, which leads to the worse classification performance. For Indian Pines and Pavia University, the window sizes in JSRC were 7×7 and 11×11 , respectively. As for the NLW-JSRC, the window sizes were set as 9×9 and 13×13 , respectively. Besides, the size of the nonlocal weighting patch was 7×7 . The parameters w_1, w_2 for the thresholds of nonlocal weights were 0.14 and 0.88, respectively. More detail was shown in [6]. All the experiments were conducted using MATLAB R2014a on a 3.2 GHz computer with 64.0 Gb RAM.

4.1 Indian Pines

The Indian Pines has 220 spectral bands ranging from 0.4-2.5 μm where each band consists of 145×145 pixels with a spatial resolution of 20m. Due to serious water absorption [13], we remove 20 absorption bands (no. 104-108, 150-163, 220) and retain only the remaining 200 bands. For this data set with 16 classes

Table 1. Sixteen classes in the AVIRIS Indian Pines data and the training and test sets for each class.

Class	Name	Train	Test
1	Alfalfa	6	40
2	Corn-notill	129	1299
3	Corn-mintill	83	747
4	Corn	24	213
5	Grass-pasture	48	435
6	Grass-trees	73	657
7	Grass-pasture-mowed	5	23
8	Hay-windrowed	48	430
9	Oats	4	16
10	Soybean-notill	97	875
11	Soybean-mintill	196	2259
12	Soybean-clean	59	534
13	Wheat	21	184
14	Woods	114	1151
15	Blgs-grass-trees-drives	39	347
16	Stone-steel-towers	12	81
Total		958	9291

Table 2. Nine classes in the ROSIS Urban Pavia University data and the training and test set for each class.

Class	Name	Train	Test
1	Asphalt	332	6299
2	Meadows	933	17716
3	Gravel	105	1994
4	Trees	154	2910
5	Painted metal sheets	68	1277
6	Bare Soil	252	4777
7	Bitumen	67	1263
8	Self-Blocking Bricks	185	3497
9	Shadows	48	899
Total		2144	40632

of land cover, we randomly select 10% of each class of samples for training and the remaining is used for testing. The reference contents are shown in Table 1 and the label map of ground truth is shown in Fig. 4(a).

The classification map was shown in Fig. 2(b)–(h) and the classification results including OA, AA, Kappa, and time were displayed in Table 3. As it shown in Table 3, all the pixel-wise methods (KNN, SVM, and SRC) had worse performance than the spectral-spatial classification methods (JSRC, NLW-JSRC, SAJSRC, and ARW-JSRC). The reason is that those pixel-wise methods can not take advantage of spatial information in HSI and avoid the “Houghes” phenomenon. HSI pixels belong to same class may have different spectral characteristic and those are same class may have the similar spectral characteristic, which brings great difficulties to those pixel-wise classification methods. Among all approaches listed at Table 3, the proposed method ARW-JSRC displays the best classification performance comparing with other methods in terms of OA, AA, Kappa. Especially, the improvement brought by ARW-JSRC on JSRC is significantly obvious in terms of various evaluation metrics. For instance, the OA

Table 3. Classification results of the Indian Pines and Pavia University, including classification accuracies for every class, AA , OA , $Kappa$, and $Time$ obtained by SVM, SRC, JSRC, NLW-JSRC, and ARW-JSRC

Class	Indian Pines					Pavia University				
	SVM	SRC	JSRC	NLW-JSRC	ARW-JSRC	SVM	SRC	JSRC	NLW-JSRC	ARW-JSRC
1	26.83	17.07	92.50	97.56	100.00	91.97	74.31	91.03	93.90	97.27
2	68.40	54.86	94.55	93.39	97.82	96.46	94.12	99.79	99.32	100.00
3	54.75	51.14	91.15	91.30	95.72	71.01	60.33	94.88	98.80	98.85
4	34.27	41.31	90.61	84.98	100.00	92.54	80.07	90.31	94.54	94.19
5	88.71	83.87	94.69	94.70	99.08	99.22	99.53	99.69	100.00	100.00
6	94.67	90.11	96.18	99.24	99.24	75.47	55.70	99.46	87.06	99.94
7	28.00	80.00	84.00	92.00	100.00	74.43	76.33	98.89	98.42	99.92
8	99.07	98.37	97.20	99.07	100.00	85.62	74.21	95.00	98.23	99.66
9	5.56	16.67	66.67	55.56	61.11	97.55	94.99	55.73	86.43	52.50
10	62.24	68.08	89.14	93.36	96.34					
11	83.34	73.25	96.42	94.84	98.82					
12	74.86	40.15	80.04	88.18	99.25					
13	95.11	90.22	91.26	97.28	99.46					
14	95.96	91.12	99.82	98.77	100.00					
15	57.93	44.96	85.63	96.54	96.83					
16	93.98	93.98	92.77	100.00	96.39					
OA	77.49	69.95	93.67	94.67	98.34	90.26	81.79	96.05	96.29	98.01
AA	66.48	64.70	90.16	92.30	96.25	87.14	78.84	91.64	95.19	93.59
Kappa	74.08	65.62	92.77	93.90	98.11	86.98	75.50	94.76	95.05	97.36
Time(s)	831.80	5.12	22.97	107.70	193.99	1403.50	26.37	190.51	574.33	1990.33

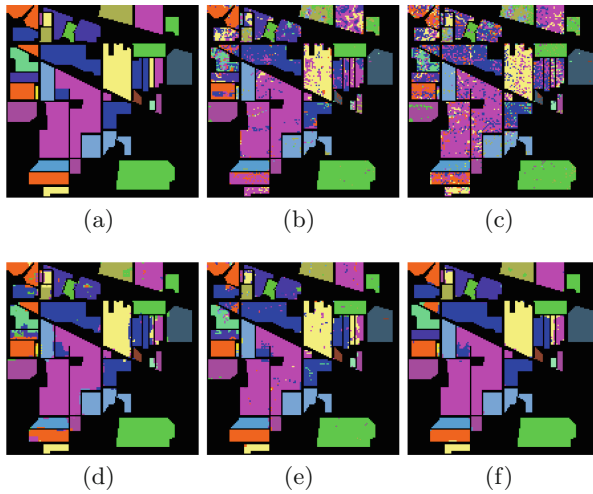


Fig. 2. Classification map for the Indian Pines image. (a) Label map; (b) SVM ($OA = 77.49\%$); (c) SRC ($OA = 69.95\%$); (d) JSRC ($OA = 93.67\%$); (e) NLW-JSRC ($OA = 93.26\%$); (f) ARW-JSRC ($OA = 98.34\%$).

has increased from 93.67% to 98.34%. Though the NLW-JSRC and SAJSRC also has improved the classification result of JSRC, the ARW-JSRC makes the great improvement on the JSRC about 5%, which is more efficient than the NLW-JSRC and SAJSRC. Moreover, the ARW-JSRC has the 100% classification accuracy in class 1, 4, 7, 8, and 14. The reason why the ARW-JSRC can make such a great improvement is that it considers the directionality of spatial structure in HSI and assigns more appropriate weights for HSI pixels in search window. However, using the rotated similar window and the nonlocal weighted based method leads to the large computation consumption for the ARW-JSRC.

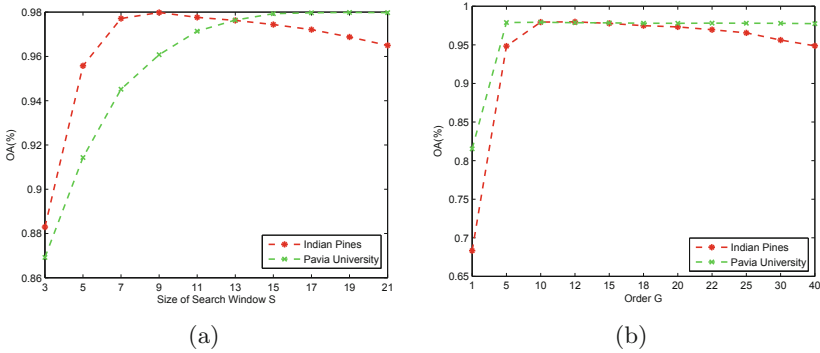


Fig. 3. Influence of parameters on classification. (a) Search window size S ; (b) Order G .

The size of search window S directly determines the size of neighborhood of the test pixel, which finally influences the joint signal matrix and the classification. The influence of search window on the classification has shown in Fig. 3(a). The size of search window S ranged from 3×3 to 21×21 . As it can be seen in Fig. 3(a), the OA increased rapidly when $3 < \sqrt{S} < 9$. The reason is that the number of HSI pixels in joint signal matrix is insufficient causing the unsatisfactory result at first. When $\sqrt{S} = 4$, the OA reaches its peak. However, the heterogenous pixels in search window will be more and more when $\sqrt{S} > 4$, which brings great challenges to the classification. Thus, once \sqrt{S} is larger than the optimal threshold, the ARW-JSRC can not solve efficiently all the heterogenous pixels in search window. In order to have the good classification performance, the size of search window S can be set as 9×9 .

The order G determines the slope of the weighed function. The influence of order G on the classification is shown in Fig. 3(b). From Fig. 3(b), it is known that the ARW-JSRC got its best OA when $G = 12$. When $1 < G < 12$, the OA rose quickly because more appropriate weights can be given by the weighed function as G grew. However, the OA decreases slow when $G > 12$. The reason is that those have small similarity may be given large weights when G is too large. Therefore, the optimal order of weighed function can be set as $G = 12$.

4.2 Pavia University

The geometric resolution of Pavia University image is 1.3 m and it has 115 bands ranging from 0.43 to 0.86 μm . Some of bands in the HSI data are noisy and we only preserve 103 bands for the experiment. For this data with 9 classes of ground truth, we randomly select 5% of each class of samples for training and the remaining is used for testing. The specific information can be seen in Table 2 and the label map of ground truth shown in Fig. 4(a).

The classification map is shown in Fig. 4(b)–(h) and the classification results can be seen in Table 3. Due to the more adequate samples than the Indian Pines, most classification algorithms have the higher OA , especially for the pixel-wise methods. Though the ARW-JSRC has the best classification performance in terms of OA , AA , and $Kappa$, it cost most time to obtain the better results. It means that the ARW-JSRC obtains the better classification result ($OA = 98.05\%$) than the JSRC ($OA = 96.05\%$) by consuming more time. As for the size of search window S and order of weighed function G , their optimal value can be set as $\sqrt{S} = 7$ and $G = 3$ from Fig. 3(a) and (b).

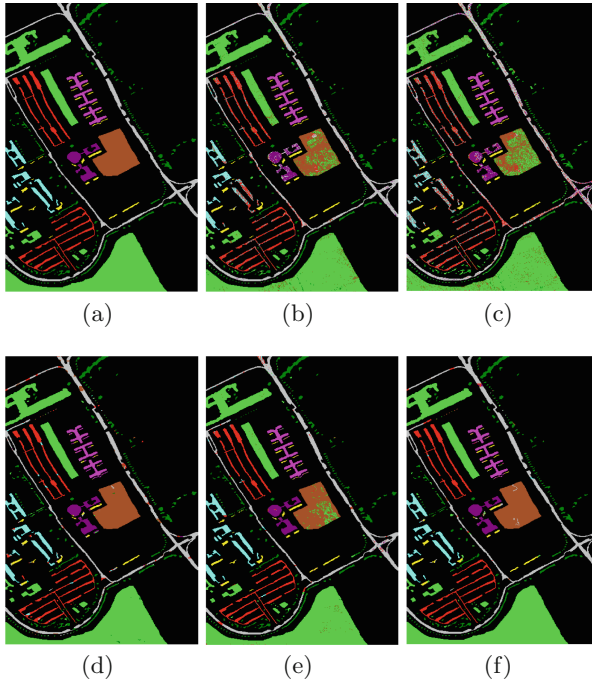


Fig. 4. Classification map for the Pavia University image. (a) Label map; (b) SVM ($OA = 90.26\%$); (c) SRC ($OA = 81.79\%$); (d) JSRC ($OA = 96.05\%$); (e) NLW-JSRC ($OA = 95.99\%$); (f) ARW-JSRC ($OA = 98.05\%$).

5 Conclusion

Aiming at the problem that JSRC can not deal with the interference of heterogeneous pixels in the search window, a joint sparse representation classification algorithm based on adaptive rotation weighting is proposed. The algorithm mainly uses the strategy of rotating similar window to measure the similarity between pixels, and uses a new method of weight calculation to assign weight to each pixel in the search window. In addition, the median of the maximum and minimum spectral angles of various training samples are used as the adaptive threshold of the weight formula. Experiments show that the proposed algorithm achieves remarkable improvement in classification accuracy.

Although the proposed method achieves good classification accuracy, it takes a heavy computation. In the future, we will start with reducing the time complexity of the algorithm and improve the efficiency of the algorithm.

References

1. Christophe, E., Leger, D., Mailhes, C., et al.: Quality criteria benchmark for hyperspectral imagery. *IEEE Trans. Geosci. Remote Sens.* **43**(9), 2103–2114 (2005)
2. Plaza, A., Benediktsson, J.A., Boardman, J.W., et al.: Recent advances in techniques for hyperspectral image processing. *Remote Sens. Environ.* (2009)
3. Landgrebe, D.: Hyperspectral image data analysis. *IEEE Signal Process. Mag.* **19**(1), 17–28 (2002)
4. Hughes, G.P.: On the mean accuracy of statistical pattern recognizers. *IEEE Trans. Inf. Theory* **14**(1), 55–63 (1968)
5. Chen, Y., Nasrabadi, N.M., Tran, T.D.: Hyperspectral image classification using dictionary-based sparse representation. *IEEE Trans. Geosci. Remote Sens.* **49**(10), 3973–3985 (2011)
6. Zhang, H., Li, J., Huang, Y., et al.: A nonlocal weighted joint sparse representation classification method for hyperspectral imagery. *IEEE J. Sel. Top. Appl. Earth Obs. Remote. Sens.* **7**(6), 2056–2065 (2014)
7. Fu, W., Li, S., Fang, L., et al.: Hyperspectral image classification via shape-adaptive joint sparse representation. *IEEE J. Sel. Top. Appl. Earth Obs. Remote. Sens.* **9**(2), 556–567 (2016)
8. Ni, D., Ma, H.: Fast classification of hyperspectral images using globally regularized archetypal representation with approximate solution. *IEEE Trans. Geosci. Remote Sens.* **55**(4), 2414–2430 (2017)
9. Bai, J., Zhang, W., Gou, Z., et al.: Nonlocal-similarity-based sparse coding for hyperspectral imagery classification. *IEEE Geosci. Remote Sens. Lett.* **14**(9), 1474–1478 (2017)
10. Gan, L., Xia, J., Du, P., et al.: Class-oriented weighted kernel sparse representation with region-level kernel for hyperspectral imagery classification. *IEEE J. Sel. Top. Appl. Earth Obs. Remote. Sens.* **11**(4), 1118–1130 (2018)
11. Leviatan, D., Temlyakov, V.N.: Simultaneous approximation by greedy algorithms. *Adv. Comput. Math.* **25**(13), 73–90 (2006)
12. Tropp, J.A., Gilbert, A.C., Strauss, M.J., et al.: Algorithms for simultaneous sparse approximation. Part I: Greedy pursuit. *Signal Process.* **86**(3), 572–588 (2006)

13. Gualtieri, J.A., Cromp, R.F.: Support vector machines for hyperspectral remote sensing classification. In: Applied Imagery Pattern Recognition Workshop, vol. 3584, pp. 221–232 (1999)
14. Melgani, F., Bruzzone, L.: Classification of hyperspectral remote sensing images with support vector machines. *IEEE Trans. Geosci. Remote Sens.* **42**(8), 1778–1790 (2004)
15. Fang, L., Wang, C., Li, S., et al.: Hyperspectral image classification via multiple-feature-based adaptive sparse representation. *IEEE Trans. Instrum. Meas.* **66**(7), 1646–1657 (2017)